



Integration of Moth Flame Optimization with Improved Firefly Algorithm in Islanded Microgrid Using Renewable Sources

Chakrapani Gandikoti^{1*} Shashank Kumar Jha¹ Bishnu Mohan Jha¹

¹Central University of Jharkhand, Cheri-Manatu, Ranchi, India

* Corresponding author's Email: Chakrapani.19210201002@cuja.ac.in

Abstract: Generally, an islanded microgrid depends on its Distributed Generators (DG) which are generally intermittent renewable energy sources such as wind turbines, photovoltaic, etc. From the various sources, effective power-sharing is required to compensate the entire microgrid demands. When there is a power outage, the existing droop methods are insufficient to operate an islanded microgrid smoothly. As a result, a hybrid optimization algorithm named Moth Flame Optimization (MFO) and Improved Firefly Algorithm (IFFA) is introduced to study the control issues of an islanded microgrid. A single battery unit is included to serve as a storage unit for intermittent sources and produce the required power when the available sources fail. Due to harmonic distortion, voltage unbalance occurs in the presence of unbalanced/non-linear loads, which can lead to voltage collapse. A comprehensive algorithm known as MFO-IFFA control is proposed to offer DC offset/steady-state error removal and fast dynamic response in an islanded microgrid. The simulation results are validated on MATLAB, which shows that the proposed MFO-IFFA achieves Total Harmonic Distortion (THD) of 1.60 % and Voltage Unbalance Factor (VUF) of 1.748 % which is much better than the existing 3IMPL and DDSRF methods.

Keywords: Battery, Distributed generators, Improved firefly algorithm, Islanded microgrid, Moth flame optimization.

Notations

Notation	Description
$P_{MPPT}(t)$	Output Power
I_M	Maximum Current
V_M	Maximum Voltage
I_{SC}	Short Circuit current
μ	Probability factor
V_{OC}	Open Circuit voltage
C_1 and C_2	Capacitances
R_1 and R_2	Resistances
G_{ref}	Reference radiation
T_c	Cell Temperature
$GT(t)$	Instance Radiation
V_{cf}	Cut off voltage
V_{ci}	Cut in Voltage
P_o	Wind Output power
P_{rs}	Power at rated speed
V_{rs}	Voltage at rated speed
V_{hub}	Height
V_0	Speed

Z_{hub}	Actual height
$SOC(t)$	Charging state
$SOC(t - 1)$	Discharging state
σ	Outflow rate
η	Efficiency
M_i	Moth
F_j	Flame
S	Spiral Path
D_i	Distance
b	Constant Value
N	Maximum Flame Count
$I(r)$	Bright Influence
γ	Light Retention coefficient
β	Firefly attraction
β_0	Engaging capability
p_i and p_j	Dual Fireflies
$p_{i,k}$	Three dimensional harmonize

1. Introduction

In a traditional grid system, with the addition of renewable energy sources to the conventional grid such as solar panels [1], wind turbines [2], the grid has to turn out to be an islanding mode [3]. Due to the connection of the utility grid, renewable sources continue to energize the distribution line feeders [4]. The situations like this put maintenance personnel at risk and make post-fault reconnection extremely difficult. This involves the establishment of a separate power entity that can accept renewable energy and storage devices that can detach from the utility grid [5]. This prevents the possibility of a tripped network containing an energized system. The centralized grid system may not always be able to provide the uninterrupted, stable electricity required by the network's sensitive loads. As a result, effective control action is essential in all conditions to provide a stable and uninterrupted power supply from the utility grid [6]. Maintaining an uninterrupted supply during a grid outage is a challenging task, sometimes it will result in an unwanted islanding effect. A redesigned method is now required to avoid the effects of islanding while yet maintaining the intended power supply [7].

When supplying loads over long distances, a traditional centralized grid system incurs a significant degree of transmission loss [8, 9]. Furthermore, the ability of renewable energy sources to collect electricity from natural resources such as solar, wind, and water has enhanced the possibility of operating a separate grid system in remote locations where conventional power generation would be unfeasible [10, 11]. Nowadays, the power quality enhancement is attracting a lot of study attention, because of the requirement for improved efficiency in electricity distribution, energy savings and operating cost reduction [12]. In a power transmission/distribution system, harmonics, reactive power, voltage sags/swells are key contributors to deteriorating the electric power quality [13]. The components such as Transformers, switchgear, relays, and motors are all affected by harmonics deviation. By injecting current harmonics and lowering grid voltage, nonlinear loads damage the electric power distribution system. According to international regulations, the power quality features should be maintained while connecting various sources into the grid [14, 15]. The proposed method is computationally simple, parallel, distributed and requires little space. Furthermore, this method seems to be preferable only if fast adaptively in a changing environment is required. This is important for exploratory data analysis since it reduces the method's computing overhead when only

a few of the independent components need to be calculated. The main contributions of this research work are given as follows:

- The proposed MFO-IFFA controller compensates the harmonics, power factor correction and distributes the energy between renewable sources
- The appropriate quantity of harmonic attenuation is determined in the suggested MFO-IFFA algorithm to meet the THD requirement.
- The proposed MFO-IFFA compensator can perform well even in the presence of noise or inter-harmonic components in the system. The MFO-IFFA compensator that has been presented can also break the resonance situation.

The organization of this research paper is presented as follows: The literature survey of existing researches related is stated in Section 2. Section 3 declared the problem statement. Section 4 stated the objectives of this research. The modelling of PV, Wind, Battery are stated in Section 5. The proposed EMS system using hybrid MFO and IFFA is discussed in Section 6. The simulation and comparative results of MFO-IFFA is presented in Section 7. Lastly, the conclusion is specified in Section 8.

2. Literature review

In [16], 3IMPL (Three Phase Improved Magnitude Phase Locked Loop) control in islanded mode has presented to achieve the proper power in a quick response. The suggested control consists of the following advantages such as eliminating DC offset, noise, and producing fast dynamic reactions under unbalancing and changes in solar insolation. A solar PV array was connected to the DC through a boost converter in the proposed microgrid, and the maximum power from the PV array was extracted using the INC (Incremental Conductance) technique. However, the total generated power is higher when the load is unbalanced, which increases the current and reduces the lifespan of the battery.

In [17], an effective EMS for a small-scale hybrid source dependent micro-grid has been demonstrated to verify the distribution system's functionality. Under various generating conditions, the major goal was to give steady power to the load. However, the demand is kept constant to observe the operation of renewable energy conversion systems and battery storage systems for various amounts of RES power generation. If there is a shift in load, this observation will be difficult to complete.

In [18], a novel Social Spider Optimizer has been proposed to compensate the load demand between hybrid renewable sources. The proposed controller comprises of PV, Wind, Diesel and Battery that control fundamental positive and negative sequence voltages independently across certain loads. Furthermore, the proposed method is used to maintain the EMS between three available resources. Installing a parallel compensator to alleviate voltage unbalance is a cost-effective solution to minimize unbalanced voltage, but, obviously increases the investment costs too.

In [19], a Novel Control Strategy has been presented for Reducing Voltage Unbalance in an Islanded Microgrid. The goal was to eliminate voltage unbalance by regulating the smallest amount of loads possible. This proposed strategy has been used to identify the bus that has the most impact on the voltage at the point of common coupling (PCC). The suggested method was used to detect the most effective bus, then the loads on that bus are managed to reduce the voltage unbalance. Power quality issues were getting increase when the microgrids were not properly managed.

In [20], A new decoupling double synchronous reference frame topology has presented for voltage imbalance compensation in microgrids. The proposed control mechanism is applied to distributed generation units with inverter interfaces. The proposed control technique was based on the decoupling double synchronous reference frame (DDSRF), which has been tweaked to make it more effective. The positive and negative sequence components can be efficiently decoupled using the improved DDSRF. In comparison to the DSRF-based control method, the suggested control delivers faster dynamic response and more effective voltage unbalance adjustment. The negative sequence component oscillation was reduced using a DDSRF-based technique. However, the oscillations were not damped.

3. Problem statement

- Temperature in the network, aging, power line topology changes, replacement, and addition of any intermediate load cause an error (change) in line impedance.
- Triple harmonics induce equipment heating and a significant level of voltage distortion due to their cumulative nature. Nonlinear loads may not be the only source of harmonics.
- In the presence of a current waveform with harmonics, voltage harmonics can be

produced by coupling impedance, filtering impedance, and other linear loads.

4. Objectives

- The goal of this study is to create control algorithms to improve the power quality of an islanded microgrid. The most essential characteristic employed by active power filters is line impedance which is applied when active power compensation is performed.
- Based on the loading condition, the suggested MFO-IFFA algorithm can prioritize harmonic compensation and voltage regulation.
- The suggested MFO-IFFA algorithm can handle line impedance mismatches and avoid harmonic current from overstressing renewable energy sources in the microgrid.
- In this research, a fast and efficient algorithm name called MFO-IFFA is introduced, which is used for phase detection. This method not only reduces the harmonics, but also performs additional functions like maximum power tracking and maintaining voltage stability.

5. Modelling of sources

5.1 PV model

The number of PV elements is selected to lower energy costs to meet the demand. PV module's output power is mostly determined by temperature, manufacturing factors, and geographic location. The voltage and capacity of a PV system are influenced by whether the PV panels are connected in series/parallel. In a PV system, MPPT is used to improve the PVs' output power. The output power $P_{MPPT}(t)$ is calculated using the following Eq. (1), which is dependent on the I_M (maximum current) and V_M (maximum voltage) (Maximum voltage).

$$P_{MPPT}(t) = I_{MPPT}(t) \times V_{MPPT}(t) \quad (1)$$

Eqs. (2) and (3) shows the MPPT current and voltage respectively.

$$I_{MPPT}(t) = I_{SC} \left\{ 1 - C_1 \left[\exp \left(\frac{V_M}{C_2 \times V_{OC}} \right) \right] \right\} + \Delta I(t) \quad (2)$$

$$V_{MPPT}(t) = V_M + \mu V_{OC} \cdot \Delta T(t) \quad (3)$$

I_{SC} states the short circuit current; probability factor is characterized by μ ; Capacitances are stated as C_1 and C_2 ; V_{OC} signifies the open circuit voltage; Maximum voltage at the model is stated as V_M ;

$\Delta T(t)$ and $\Delta I(t)$ are stated as change in temperature and current. From the Eqs. (2) and (3), Eqs. (4) to (7) are derived.

$$C_1 = \left(1 - \frac{I_M}{I_{sc}}\right) \times \exp\left(-\frac{V_M}{c_2 \times V_{OC}}\right) \quad (4)$$

$$C_2 = \left(\frac{V_M}{V_{OC}} - 1\right) \times \left[\ln\left(1 - \frac{I_M}{I_{sc}}\right)\right]^{-1} \quad (5)$$

$$\Delta I(t) = I_{sc} \left(\frac{GT(t)}{G_{ref}} - 1\right) + \alpha_{1,sc} \times \Delta T(t) \quad (6)$$

$$\Delta T(t) = T_c(t) - T_{c,ref} \quad (7)$$

Where, determined current is stated as I_M ; $GT(t)$ signifies the instance radiation; reference radiation is stated as G_{ref} ; T_c and $T_{c,ref}$ states the cell temperature and its standard reference conditions.

5.2 Wind turbine model

The output of Wind turbine is primarily determined by the parameters such as elevation, esteemed dimensions and rapidity. The voltage at rated speed (V_{rs}), cut off voltage (V_{cf}), and cut in voltage (V_{ci}) are all aspects of wind speed. The output power of wind is specified along with the boundary conditions in Eq. (8).

$$P_o = P_{rs} \left\{ \begin{array}{ll} 0 & V < V_{ci} \\ a \times V^3 - b \times P_{rs}, & V_{ci} < V < V_{rs} \\ 1 & V_{rs} < V < V_{cf} \end{array} \right\} \quad (8)$$

The boundary conditions of wind are mainly based on speed and height. According to wind shield, the wind speed is not stable and changing with respect to height. Here, a wind speed of 14 metre per second is calculated with atmospheric boundary layer height of 1000 metres. P_o and P_{rs} are signified as output power and power at rated speed; where $a = P_{rs}/(V_{rs}^3 - V_{ci}^3)$ and $b = V_{ci}^3/(V_{rs}^3 - V_{ci}^3)$. The wind speed measurements are represented in Eq. (9).

$$V_{hub} = V_0 \times \left(\frac{Z_{hub}}{Z_0}\right) \times \alpha \quad (9)$$

Where V_{hub} states the height; V_0 signifies the reference speed; Z_{hub} represents the actual height; Z_0 states the speed limit and power is characterized as α .

5.3 Battery model

The battery's charging and discharging conditions are represented in Eqs. (10) and (11). The battery is charged when the solar and wind exceeds the demand. The process of discharge happens when the load exceeds the RES power levels.

$$SOC = SOC(t-1) \times (1 - \sigma) + [P_{RES}(t) - P_L(t)/\eta_{inv}] \times \eta_{ch} \quad (10)$$

$$SOC = SOC(t-1) \times (1 - \sigma) + [P_L(t)/\eta_{inv} - P_{RES}(t)] \times \eta_{disch} \quad (11)$$

SOC and $SOC(t-1)$ represents the charging and discharging conditions of the battery. The outflow rate is stated as σ . P_{RES} and P_L stand for power from RES and power from the load. η_{inv} , η_{ch} and η_{disch} are the efficiency symbols for the inverter, charging, and discharging states, respectively.

6. Proposed method

In this research, a hybrid MFO-IFFA approach is proposed for islanded microgrid power networks. The goal is to eliminate voltage unbalance by controlling the smallest amount of loads possible. The proposed MFO-IFFA is the most suitable method to identify the bus that has the most impact on the voltage at the Point of Common Coupling (PCC). In the analysis of transmission and distribution networks, voltage is one of the user variables. The proposed MFO-IFFA investigates the change in the voltage value of the buses after a load or generation change occurs in the system. MFO-IFFA method has become more important in recent years, especially a renewable source is added to the distribution grid. This method identifies the buses that have the highest sensitivity values and connects the sources that will improve the grid's stability and power quality.

6.1 Moth flame optimization

Moths attempt to form stable points with neighbouring light sources by coming closer in a twisting path. The moths address the arrangement in computation, whereas their location in space addresses the flexibility of the issue in which it has been used. MFO first generates fitness values for each moth by randomly creating moths within the solution space. The flame is then used to mark an ideal spot. The location update of the moths is defined by the spiral movement function. This position update is utilized to acquire the flame's optimal location, and the MFO is updated with a new best individual location. The MFO performs the same

procedures as the moth's location update and new location generation.

Every moth's fitness function is recorded in an array that is arranged in matrix form and intended for storing analogous criteria that are similarly described by an array. Formerly, a subsequent function is used to construct the moth position which is expressed in Eq. (12).

$$M_i = S(M_i, F_j) \quad (12)$$

If M_i characterizes the i^{th} Moth, j^{th} flame is designated by F_j and function of a spiral path is stated as S . Deliberating the aforementioned state, the moth route is described as subsequent Eq. (13),

$$S(M_i, F_j) = D_i \cdot e^{bt} \cdot \cos(2\pi t) + F_j \quad (13)$$

Where distance amongst the i^{th} moth and j^{th} flame of problematics are signified as D_i . Constant values are stated as b that support the outline of the curved route and t diverge in the range of -1 and 1 indiscriminately. Supplementary D_i is designed as in Eq. (14),

$$D_i = |F_j - M_i| \quad (14)$$

In Eq. (3), M_i represents i^{th} Moth, F_j represents j^{th} flame and D_i signifies distance amongst the nodes. Through the usage aforementioned equivalence, the moth location is restructured all over the flame. The population gets diminished through the repetition count using flame. Those formulations are mentioned in Eq. (15),

$$\text{Flame no} = \text{round} \left(N - 1 * \frac{N-1}{T} \right) \quad (15)$$

Where N denotes the maximum flame count and T represents the maximum iterations count.

6.2 Firefly algorithm

The Firefly Algorithm (FA) is an arbitrary inquiry calculation based on swarm intelligence that simulates the attraction instrument amongst various fireflies in the surroundings. The following glorification standards are used to appreciate specific features of fireflies while building numerical models of FA:

- Regardless of female, all fireflies are intrigued by the light strength among clusters;

- The fascination of fireflies to one another corresponds to light splendour;
- The splendour of fireflies is associated with fixed capacity values.

Author Yang advanced analysis through individualities of fireflies to achieve improved execution which is the major shortcomings of ordinary fireflies. The FA results show that it can effectively address a certain type of global streamlining issue. For example, FA was successfully used to a global development issue involving a tension funneling plan. In certain cases, the firefly boundaries are determined ahead of time which causes premature convergence and inability to combine boundary sets. The standard FA should be upgraded in the future to achieve greater advanced execution.

6.2.1. Improved firefly algorithm

By investigating the firefly boundaries, light retention coefficient γ is excessively huge and it operates as a decent value. Every firefly contains bright influence $I(r)$ which is written in Eq. (16)

$$I(r) = I_0 e^{-\gamma r^m} \quad m \geq 1 \quad (16)$$

So, firefly attraction β can diverge conferring to the calculation assumed through Eq. (17),

$$\beta(r) = \beta_0 e^{-\gamma r^m} \quad m \geq 1 \quad (17)$$

where β_0 signifies the greatest engaging quality (at $r = 0$) and γ is the light assimilation constant, which regulates the diminishing of the light power. The expanse amongst dual fireflies i and j at p_i and p_j locations are considered as Eq. (18).

$$r_{ij} = |p_i - p_j| = \sqrt{\sum_{k=1}^l p_{i,k} - p_{j,k}^2} \quad (18)$$

Where $p_{i,k}$ is three-dimensional harmonize p_i . The effort is defined in Eq. (19).

$$p_i = p_i + \beta_0 e^{-\gamma r_{ij}^2} (p_i - p_j) + \alpha (\text{rand} \frac{1}{2}) \quad (19)$$

Where the initial term is the current situation of a firefly i (p_i is the arrangement of a firefly). At every iterative advance, the splendor and the engaging quality of every firefly are registered. The intelligence of every firefly is discriminated and the

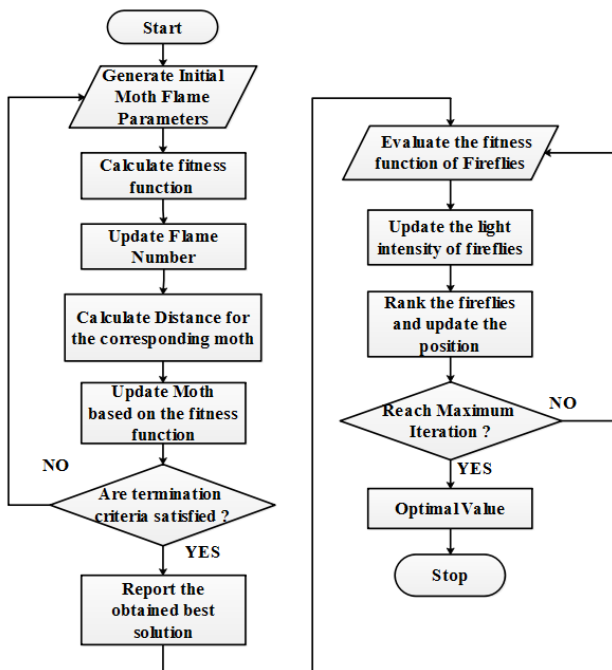


Figure. 1 Flowchart for the proposed method

location of remaining fireflies is refreshed utilizing condition Eq. (19).

The flowchart for the suggested method is shown in Fig. 1. For various loading situations and harmonic levels, the compensatory impedance is designed using the MFO-IFFA control. Due to the impedance mismatch, the stress increases on the inverter as well as the switches, which will cause severe damage during heavy loading situations. In that instance, the adaptive method will widen the gap between the estimated and virtual impedances. In the same way, as the harmonic level rises, the inverter will automatically increase the difference between the estimated and virtual impedance which reduces the stress on the switches. The proposed MFO-IFFA controller emphasizes voltage management and better THD at the coupling point under low harmonic loading circumstances. Individual harmonics are evaluated and achieved at the appropriate level using the individual harmonic compensator which is operated through the proposed MFO-IFFA controller. The proposed MFO-IFFA controllers are applied for phase detection and harmonic component estimation. The harmonics elimination block removes all even and odd harmonics from the input current, resulting in a PLL waveform that is harmonic free. The harmonic estimation block estimates the fundamental and individual harmonic components at the same time. The impedance compensation block uses these approximated values.

7. Result and discussion

MATLAB software is utilized in this study to validate the results. The MFO-IFFA controller is implemented and simulated in the grid-connected RES using MATLAB R2018a, which runs on a Windows 8 operating system with an Intel Core i3 processor and 4GB RAM. The inverters using the suggested control algorithms are simulated using the SimPowerSystems package. Each of the following sections explains the topology utilized in the simulations. The proposed MFO-IFFA is evaluated in simulations to verify the compensatory effect of the proposed control strategy on the negative sequence voltage. Tables 1 and 2 illustrate the parameters of the microgrid power stage. Furthermore, both DGs have the same converter side filter inductor and capacitor, but the grid-side filter inductor and low voltage feeder are different. In this section, the findings of two situations with various grid-side filter inductors are reported. In some cases, the simulation includes a standard grid-side filter inductor. To demonstrate the compensatory impact of the proposed control technique, the large scale grid-side filter inductor is introduced to provide greater negative sequence voltage drop.

Fig. 2 depicts the proposed model in Simulink. Here, the physical parameter model is obtained for the designed model. The ideal model of bidirectional DC-DC converter is considered for simplifying the complexity of modelling. The Simulink model is made with PV, Wind and energy storage battery through 8 n-channel MOSFETs and 8 diodes, capacitors, inductors and resistances. The frequency and line voltage are then gradually increased to 60Hz and 600V, respectively. The switching harmonics are partially cancelled, once the carrier phase of the inverter is set to +90.

Table 1. Simulation specifications

Control Parameter	$\mu 1=67, \mu 2=13333, \mu 3=0.01$ and $\mu 4=25$
Interfacing inductors and R C ripple filter	$L_f=6\text{mH}, 5\text{ ohm} \ \& \ 10\mu\text{F}$ respectively
Lead acid BES	253 V, 35Ah.
Nonlinear Load	$R = 14.7\text{ ohms}, L = 100\text{ mH}.$
Solar Photovoltaic Array	$V_{oc}=390\text{ V}, I_{sc}=5\text{ A}, V_{pvmp}=335.87\text{ V}, I_{pvmp}=4.74\text{ A}$ and $P_{mp}=1585\text{ W}.$
Wind Generator	Three phase 380V, 3.7kW, 4 Poles, 50Hz, Star Connected In delta connection line voltage is 220V

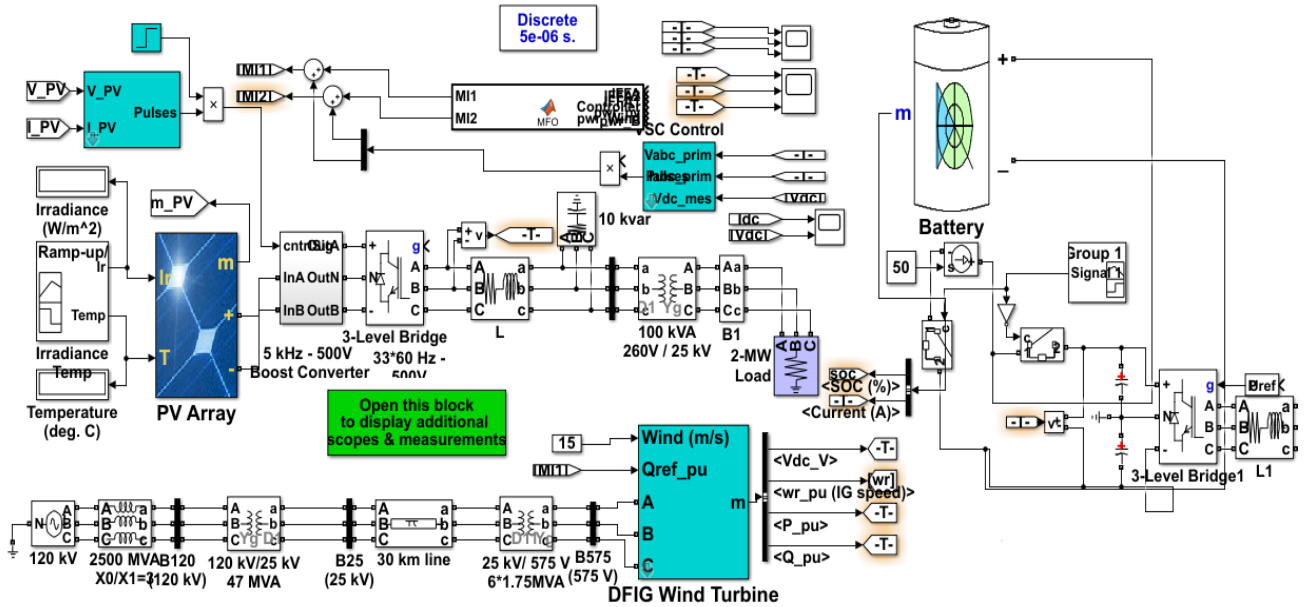


Figure. 2 Simulink view of the proposed model

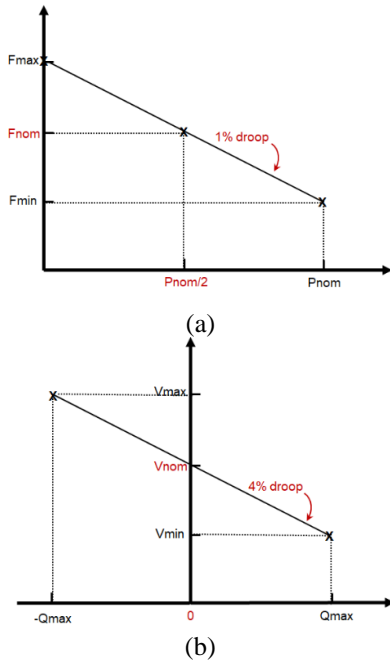


Figure. 3 (a) droop control (1%) and (b) droop control (4%)

The proposed method's droop characteristics are shown in Fig. 3. The droop P/F is set to 1%, allowing the microgrid frequency to range between 60.3 Hz to 59.7 Hz. The droop Q/V is adjusted to 4%, allowing the microgrid voltage at the PCC bus to range between $612 V_{rms}$ to $588 V_{rms}$. The measuring subsystem calculates the active and reactive power generated by the inverter based on the frequency value provided by the Droop control. The dq components of the three-phase voltages and currents at the microgrid PCC bus are also computed. The Voltage Regulators receive the reference voltage V_{ref} from the Droop Control. The reference currents

I_{dref} and I_{qref} are generated by the regulators using the measured dq voltages and the reference voltage V_{ref} . Current Regulators are supplied the I_{dref} and I_{qref} reference currents. The regulators use the measured and reference currents to generate the inverter's needed dq voltages. The scaled and transformed $V_d V_q$ signals are fed into the PWM modulator, which generates pulses for the inverter.

7.1 Performance analysis

In grid-connected RES, the performance of the MFO-IFFA controller is assessed through various performance measures. Three integrated controllers, MFO, IFFA, MFO-FFA, and MFO-IFFA, are used to test the MFO-IFFA controller.

7.1.1. MPPT current and voltage

The MPPT voltage and current findings are shown in Fig. 4 and 5, respectively. The voltage and

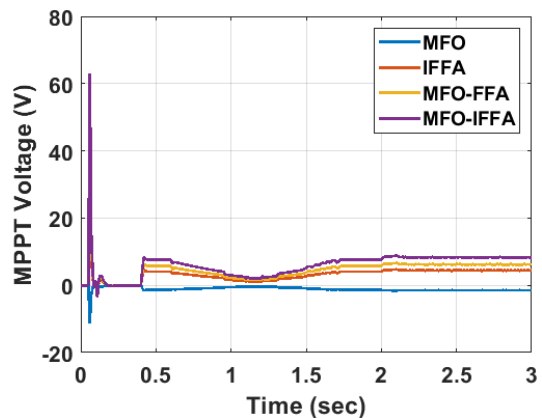


Figure. 4 Voltage on MPPT

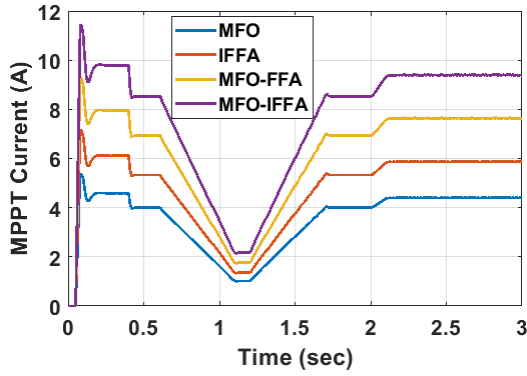


Figure. 5 Current on MPPT

current of the MFO-MPPT IFFA are compared to three other controllers: MFO, IFFA, and MFO-FFA. The MPPT performance of the PV module embedded in the grid-connected RES is assessed. As demonstrated in the figures, the proposed MFO-IFFA controller outperforms the other three controllers in terms of MPPT performance. MFO, IFFA, and MFO-FFA controllers have lower power than proposed MFO-IFFA controllers. Fig. 4 and 5 illustrates that the proposed MFO-IFFA controller has higher MPPT current/voltage values and improved the system's performance in both stable and dynamic states.

7.1.2. Grid voltage and grid current

Fig. 6 shows the graphical illustration of grid voltage and Fig. 7 depicts the grid voltage provided between 0.92s and 1.04s. Fig. 7, clearly shows that

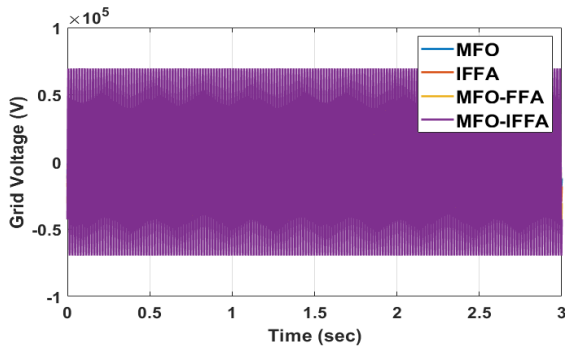


Figure. 6 Grid voltage

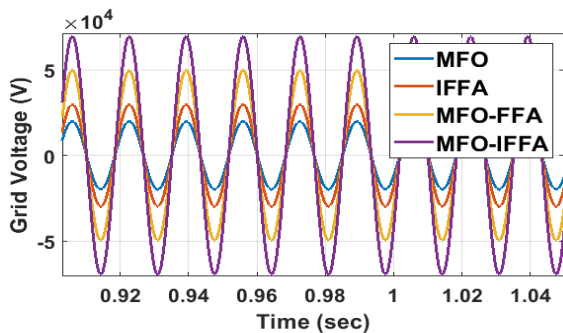


Figure. 7 Grid voltage between 0.92s and 1.04s

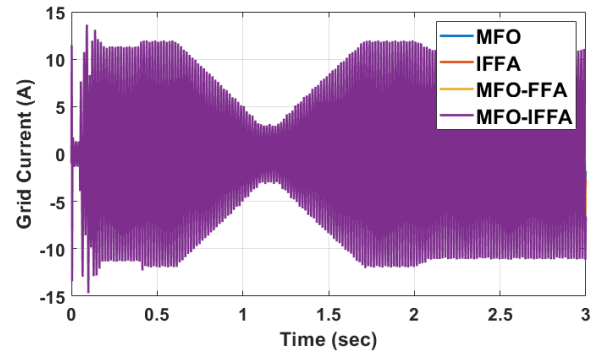


Figure. 8 Grid current

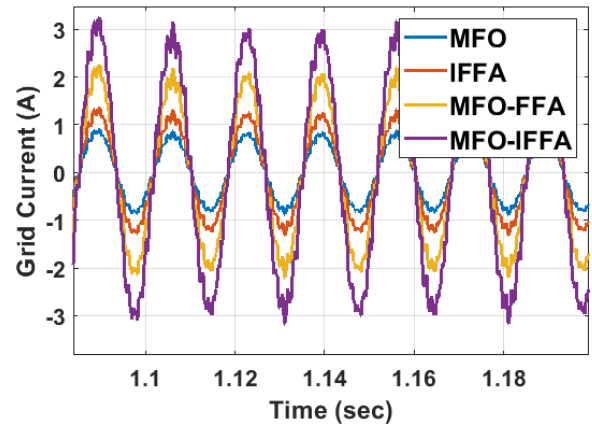


Figure. 9 Grid current between 1.09s and 1.19s

the proposed MFO-IFFA produces greater voltage while related to conventional approaches for compensating for demand. The zoom aspects of grid current with the proposed approach are shown in Fig. 8 and 9.

7.1.3. Real and Reactive power

The real power and reactive power established through utility grid are depicted in Fig. 10 and 11, respectively. From the figures, it clearly shows that the MFO-IFFA controller is higher than existing methods as shown in Fig. 10 and 11. As a result, the proposed MFO-IFFA controller meets the grid's higher energy demand.

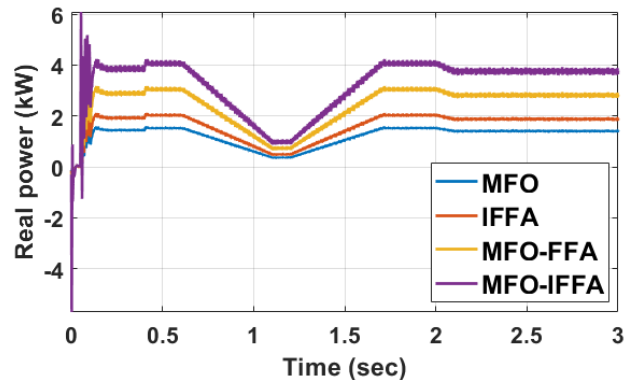


Figure. 10 Real power

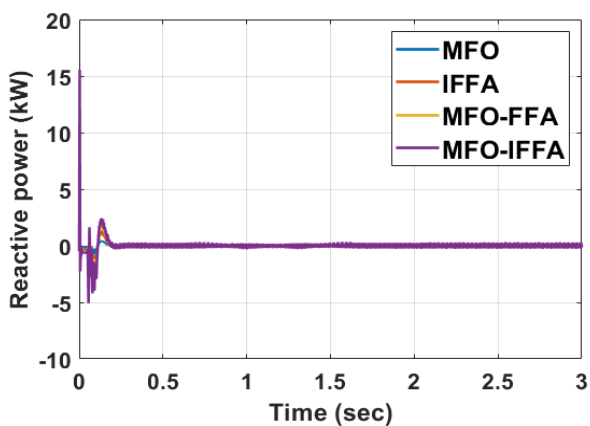


Figure. 11 Reactive power

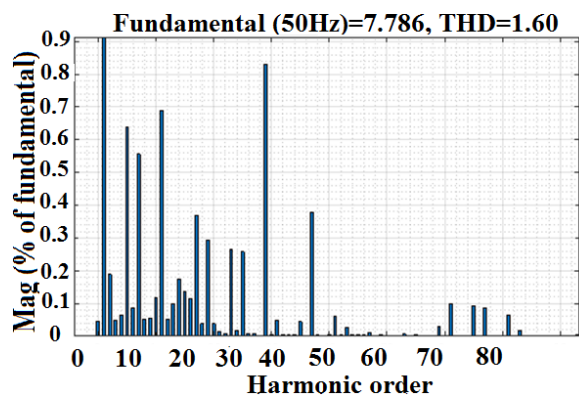


Figure. 12 FFT analysis

7.2 Comparative analysis

By comparing the system with the MFO-IFFA to previous RES designs, the effectiveness of the system with the MFO-IFFA is validated. To demonstrate the originality of control algorithms, the proposed MFO-IFFA control is compared to the existing LMS (Least Mean Square) and SOGI (Second Order Generated Integral) controllers, 3IMPL [16] and 3MPLL [16]. Table 2 shows the comparative analysis of THD.

The comparative analysis of THD is tabulated in Table 2. When the phase 'a' of the load is eliminated, the harmonics are present in the magnitude component of control algorithms when the input signal contains both DC offset and noise. On the other hand, the proposed MFO-IFFA control estimates less harmonics which is illustrated in Fig. 12. Whereas, Fig. 13 shows the Graphical illustration of THD comparison.

Table 3 shows the comparative analysis of Voltage Unbalance Factor (VUF). Fig. 14 shows the graphical illustration of VUF. Fig. 14, clearly shows that the proposed MFO-IFFA achieves a better VUF of 1.748% which is less when compared with existing DDSRF [20] and modified DDSRF [20] methods.

Table 4 shows the comparative analysis of hybrid renewable sources with existing MPPT method [17].

Table 2. Comparative analysis of THD

Techniques	THD (%)
BPF	5
LMS	6
SOGI	4
3MPLL [16]	4.8
3IMPL [16]	3
Proposed MFO-IFFA	1.60

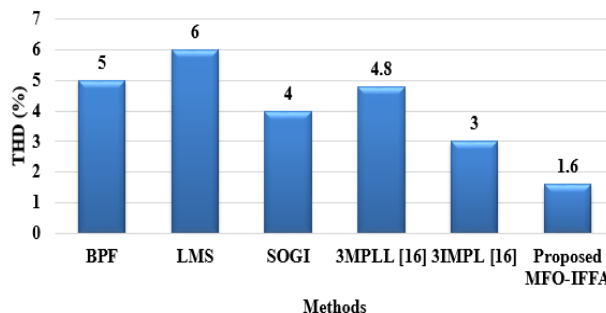


Figure. 13 Graphical illustration of THD comparison

Table 3. Comparison of voltage unbalance factor

Method	VUF (%)
DDSRF [20]	5.591
Modified DDSRF [20]	2
Proposed MFO-IFFA	1.748

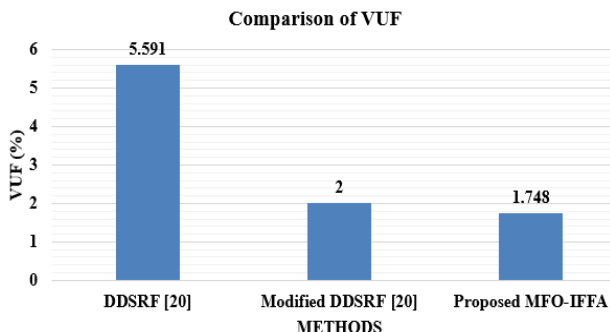


Figure. 14 Graphical illustration of VUF comparison

From the Table 4, it clearly shows that proposed MFO-IFFA achieves higher power when compared with existing MPPT in all the hybrid renewable sources. The computational time of each approach is an important issue that is considered in the analysis. Table 5 shows the computational time analysis for existing methods such as Harris Hawks Optimizer (HHO), Grey Wolf Optimizer (GWO), Social Spider Optimizer (SSO) with proposed MFO-IFFA. On the other hand, HHO employs renewable sources with a computational time of 10416.69 sec, where GWO attains at 4546.36 sec and SSO attains at 4497.32 sec. From the table 5, it obviously shows that proposed MFO-IFFA achieves better computational time of 4362.91 sec which is better than existing HHO, GWO & SSO [18] methods.

Table 4. Comparison analysis of power

Environmental Conditions	Time (Min)	PV Power (W)		Wind Power (W)		Battery Power (W)	
		Existing MPPT [17]	Proposed MFO-IFFA	Existing MPPT [17]	Proposed MFO-IFFA	Existing MPPT [17]	Proposed MFO-IFFA
PV Irradiation – 1000 Temperature – 35° Wind Speed – 9 m/s Pitch angle gain – 5 Nominal power - 50×103 Max. pitch angle – 45°	0	50	63.79	35	43.22	2	15.02
	10	54.26	65.24	42.18	45.13	-22.2	1.09
	20	54.26	66.08	42.18	47.91	-43.14	0.72
	30	54.26	68.27	42.18	49.19	-43.14	2.01
	40	54.26	70.75	42.18	51.93	-22.17	1.04
	50	54.26	71.54	42.18	51.93	2.9	3.22
	60	54.26	71.54	42.18	51.93	16.13	19.03
	70	54.26	71.54	42.18	51.93	22.24	24.07

Table 5. Comparison of computational time

Methods	Computational Time (sec)
HHO [18]	10416.69
GWO [18]	4546.36
SSO [18]	4497.32
Proposed MFO-IFFA	4362.91

8. Conclusion

In this research, the problem of unbalanced voltage compensation in a three-phase island microgrid system is analysed with an MFO-IFFA controller. The proposed MFO-IFFA control technique has unique qualities such as harmonic removal, reactive power compensation, and load balancing. The frequency domain of the proposed controller is constructed in the stationary frame, but the major importance of the proposed controller is that does not require a sequence separation process. The simulation results, clearly show that the proposed MFO-IFFA achieves a lower THD of 1.60 % and a higher VUF of 1.748 % than the existing 3IMPL and DDSRF approaches. The simulation results show that the suggested control mechanism effectively compensates for voltage unbalance and that the load current is distributed evenly amongst the DGs. In the future, this research can be prolonged with different types of loads with different conditions to analyse the voltage unbalance features.

Conflicts of Interest

The authors declare no conflict of interest.

Author Contributions

The paper background work, conceptualization, methodology, dataset collection, implementation, result analysis and comparison, preparing and editing draft, visualization have been done by first and

second author. The supervision, review of work and project administration, have been done by third author.

References

- [1] T. Nguyen, H. Yoo, H. Kim, and H. N. Duc, "Direct phase angle and voltage amplitude model predictive control of a power converter for microgrid applications", *Energies*, Vol. 11, No. 9, p. 2254, 2018.
- [2] Q. Liu, Y. Tao, X. Liu, Y. Deng, and X. He, "Voltage unbalance and harmonics compensation for islanded microgrid inverters", *IET Power Electronics*, Vol. 7, No. 5 pp. 1055-1063, 2014.
- [3] Y. Han, P. Shen, X. Zhao, and J. M. Guerrero, "An enhanced power sharing scheme for voltage unbalance and harmonics compensation in an islanded AC microgrid", *IEEE Transactions on Energy Conversion*, Vol. 31, No. 3, pp. 1037-1050, 2016.
- [4] A. Ranjbaran and M. Ebadian, "A power sharing scheme for voltage unbalance and harmonics compensation in an islanded microgrid", *Electric Power Systems Research*, Vol. 155, pp. 153-163, 2018.
- [5] F. Guo, C. Wen, J. Mao, J. Chen, and Y. D. Song, "Distributed cooperative secondary control for voltage unbalance compensation in an islanded microgrid", *IEEE Transactions on Industrial Informatics*, Vol. 11, No. 5, pp. 1078-1088, 2015.

- [6] M. Savaghebi, A. Jalilian, J. C. Vasquez, and J. M. Guerrero, "Secondary control scheme for voltage unbalance compensation in an islanded droop-controlled microgrid", *IEEE Transactions on Smart Grid*, Vol. 3, No. 2, pp. 797-807, 2012.
- [7] S. Acharya, M. S. E. Moursi, A. A. Hinai, A. S. A. Sumaiti, and H. H. Zeineldin, "A control strategy for voltage unbalance mitigation in an islanded microgrid considering demand side management capability", *IEEE Transactions on Smart Grid*, Vol. 10, No. 3, pp. 2558-2568, 2018.
- [8] L. Meng, X. Zhao, F. Tang, M. Savaghebi, T. Dragicevic, J. C. Vasquez, and J. M. Guerrero, "Distributed voltage unbalance compensation in islanded microgrids by using a dynamic consensus algorithm", *IEEE Transactions on Power Electronics*, Vol. 31, No. 1, pp. 827-838, 2015.
- [9] B. Ren, X. Sun, S. Chen, and H. Liu, "A compensation control scheme of voltage unbalance using a combined three-phase inverter in an islanded microgrid", *Energies*, Vol. 11, No. 9, p. 2486, 2018.
- [10] S. Hoseinnia, M. Akhbari, M. Hamzeh, and J. M. Guerrero, "A control scheme for voltage unbalance compensation in an islanded microgrid", *Electric Power Systems Research*, Vol. 177, No. 1, p. 106016, 2019.
- [11] M. Savaghebi, A. Jalilian, J. C. Vasquez, and J. M. Guerrero, "Autonomous voltage unbalance compensation in an islanded droop-controlled microgrid", *IEEE Transactions on Industrial Electronics*, Vol. 60, No. 4, pp. 1390-1402, 2012.
- [12] L. Meng, F. Tang, M. Savaghebi, J. C. Vasquez, and J. M. Guerrero, "Tertiary control of voltage unbalance compensation for optimal power quality in islanded microgrids", *IEEE Transactions on Energy Conversion*, Vol. 29, No. 4, pp. 802-815, 2014.
- [13] Y. Peng, Z. Shuai, J. M. Guerrero, Y. Li, A. Luo, and Z. J. Shen, "Performance improvement of the unbalanced voltage compensation in islanded microgrid based on small-signal analysis", *IEEE Transactions on Industrial Electronics*, Vol. 67, No. 7, pp. 5531-5542, 2019.
- [14] S. Ghosh and S. Chattopadhyay, "Correction of line-voltage unbalance by the decentralized inverters in an islanded microgrid", In: *Proc. of IEEE Applied Power Electronics Conference and Exposition*, pp. 622-628, 2020.
- [15] M. Savaghebi, A. Jalilian, J. C. Vasquez, and J. M. Guerrero, "Secondary control for voltage quality enhancement in microgrids", *IEEE Transactions on Smart Grid*, Vol. 3, No. 4, pp. 1893-1902, 2012.
- [16] R. Sharma, S. Kewat, and B. Singh, "Robust 3IMPL control algorithm for power management of SyRG/PV/BES-based distributed islanded microgrid", *IEEE Transactions on Industrial Electronics*, Vol. 66, No. 10, pp. 7765-7777, 2018.
- [17] P. S. Kumar, R. P. S. Chandrasena, V. Ramu, G. N. Srinivas, and K. V. S. M. Babu, "Energy management system for small scale hybrid wind solar battery based microgrid", *IEEE Access*, Vol. 8, pp. 8336-8345, 2020.
- [18] A. Fathy, K. Kaaniche, and T. M. Alanazi, "Recent approach based social spider optimizer for optimal sizing of hybrid PV/wind/battery/diesel integrated microgrid in aljouf region", *IEEE Access*, Vol. 8, pp. 57630-57645, 2020.
- [19] S. E. Kavitha and G. M. Kumar, "A Novel Control Strategy for Reduce Voltage Unbalance in an Islanded Microgrid", *International Research Journal of Engineering and Technology*, Vol. 08, No. 5, pp. 2984-2989, 2021.
- [20] M. Ahmadi and S. Karimi, "Voltage unbalance compensation using new structure of decouple double synchronous reference frame in stand-alone microgrids", *IET Generation, Transmission & Distribution*, Vol. 14, No. 22, pp. 5093-5103, 2020.